



ends of the same chain, i.e. the value  $(M - m)/M$  should be small, otherwise analogical to Fresnell reflection effects [20] will take place and one has to take into account both reflection and tunneling processes, that makes difficult clear identification of manifestations of LZ tunneling.

By introducing dimensionless time variable and re-defining parameters it is possible to choose  $m_0 = k_1 = 1$ . Working in this setup we are seeking the solution in the form of slow space-time modulation of plane waves:

$$\begin{aligned} u_n &= \frac{A(\xi, \epsilon n)}{2} e^{i(\omega t - pn)} + c.c., \\ w_n &= \frac{B(\xi, \epsilon n)}{2} e^{i(\omega t - pn)} + c.c., \quad \xi = \epsilon(n - vt) \end{aligned} \quad (4)$$

where  $\epsilon \ll 1$  is a small expansion parameter. Collective slow variable  $\xi$  has been introduced and  $v = d\omega/dp = \sin p/\omega$  stands for a group velocity. Now we suppose that  $\alpha n \lesssim \epsilon$ ,  $k \sim \epsilon$  and  $k_3 \sim \epsilon$ . Then in the zero approximation over  $\epsilon$  substituting (4) into (13) and (14) one automatically gets dispersion relation for plane waves  $\omega^2 = 2(1 - \cos p)$ . While in the next approximation over  $\epsilon$  making simple phase modification for  $A$  and  $B$  we obtain following equations:

$$-i \frac{\partial A}{\partial n} = \alpha' n A - \kappa B + 2r|A|^2 A, \quad (5)$$

$$-i \frac{\partial B}{\partial n} = -\alpha' n B - \kappa A + 2r|B|^2 B \quad (6)$$

with gradient coefficient  $\alpha' = \omega^2 \alpha / (2 \sin p)$ , coupling constant  $\kappa = k / (2 \sin p)$  and nonlinearity  $r = 3k_3(\cos p - 1)^2 / (4 \sin p)$ . Substituting  $A \sim e^{i\beta n}$  and  $B \sim e^{i\beta n}$  into (5) and (6) it is easy to determine adiabatic levels  $\beta$  for fixed  $n$  and one obtains quartic equation:

$$(\alpha' n \beta)^2 = (\beta^2 - \kappa^2)(r\mathcal{F} - \beta)^2 \quad (7)$$

where  $\mathcal{F}(\xi) = |A|^2 + |B|^2$  is a conserved quantity for fixed  $\xi$ .

In case of vanishing nonlinearity  $k_3 \rightarrow 0$  ( $r \rightarrow 0$ ) equations (5) and (6) reduce exactly to Landau-Zener model [1] in the spatial domain. In the same limit, (7) gives symmetric adiabatic levels  $\beta = \pm \sqrt{\kappa^2 + (\alpha' n)^2}$  displayed in Fig. 2 c), e). According to general LZ formula [1], having at  $n \rightarrow -\infty$  the values  $A = 1$  and  $B = 0$ , transition probability is expressed as

$$P = \exp\left(-\frac{\pi \kappa^2}{\alpha'}\right) = \exp\left(-\frac{\pi k^2}{2\omega^2 \alpha \sin p}\right). \quad (8)$$

In particular, this means that if according to (4) one has modulated plane wave distribution at fixed  $\xi = \xi_0$  and  $n = -\infty$  such that  $A(\xi = \xi_0, n = -\infty) = A_0$ ,  $B(\xi = \xi_0, n = -\infty) = 0$ , then formula (7) allows to construct the tunneling amplitudes at  $n = \infty$  and the same  $\xi = \xi_0$  as follows:  $|A(\xi = \xi_0, n = \infty)|^2 = P|A_0|^2$  and  $|B(\xi = \xi_0, n = \infty)|^2 = (1 - P)|A_0|^2$ .

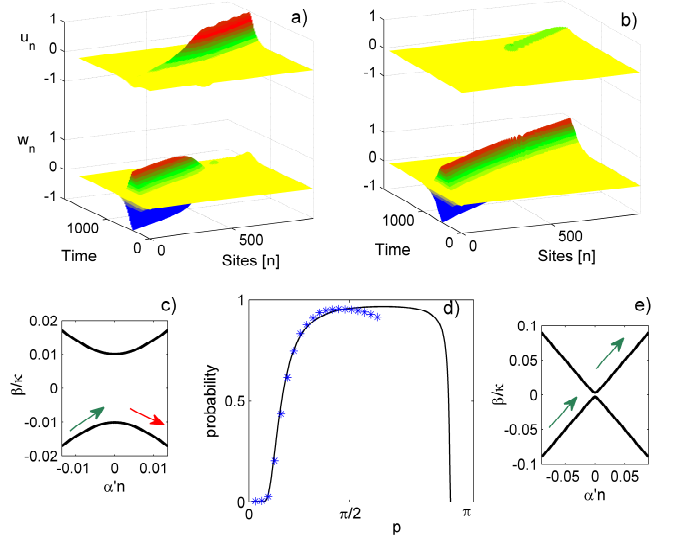


FIG. 2: result of numerical simulation on the initial model system (13), (14) in linear limit with mass distribution (3) presented schematically in Fig. 1. Upper surface plots a) and b) represent linear wavepacket dynamics injected into the lower chain. Carrier wavenumbers are  $p = 0.3$  and  $p = \pi/2$  in a) and b) graphs, respectively. Graph d) displays analytical dependence of tunneling probability on carrier wavenumber given by LZ formula (8) (solid curve) while stars are results of numerical simulations. Graphs c) and d) represent adiabatic and diabatic regimes in linear limit  $k_3 \rightarrow 0$  corresponding to the cases in the surf plots a) and b) respectively. We use the following parameters for the simulations and comparison: keeping intrachain coupling constant equal to unity we choose interchain coupling as  $k = 0.006$  and gradient coefficient as  $\alpha = 6.5 \cdot 10^{-4}$ . Masses at ultimate ends of the ladder are fixed as  $m = 1.09$  and  $m = 0.91$ .

As a result, taking initially some localized wavefunction of collective variable  $\xi$ , the wave will propagate through tunneling region and at the output the amplitudes should follow to LZ transition probability formula (7). Particularly, we inject at the input modulated wave via oscillating ultimate left end of the ladder as follows  $u_0(t) = \cos(\omega t)/\cosh(t/L)$ ,  $w_0(t) = 0$  or  $u_0(t) = 0$ ,  $w_0(t) = \cos(\omega t)/\cosh(t/L)$  with  $L = 80$  ( $L$  should be large in order to have small spreading effects) and monitor wavepacket amplitudes in both chains at the output. Fig. 2 shows that in the range  $0 < p \lesssim \pi/2$  numerical experiment almost repeats theoretical curve of the dependence of tunneling probability on the carrier wavenumber of the injected wave-packet  $p$  (see Fig. 2 d). Particularly, the process is strongly symmetric, i.e. injecting the wavepacket into upper (lower) chain and keeping pinned lower (upper) chain, tunneling characteristics for both processes are exactly the same as it should follow from original LZ model. On the other hand, changing carrier wavenumber of the injected wavepacket from  $p = 0.3$  to  $p = \pi/2$  one monitors transition from

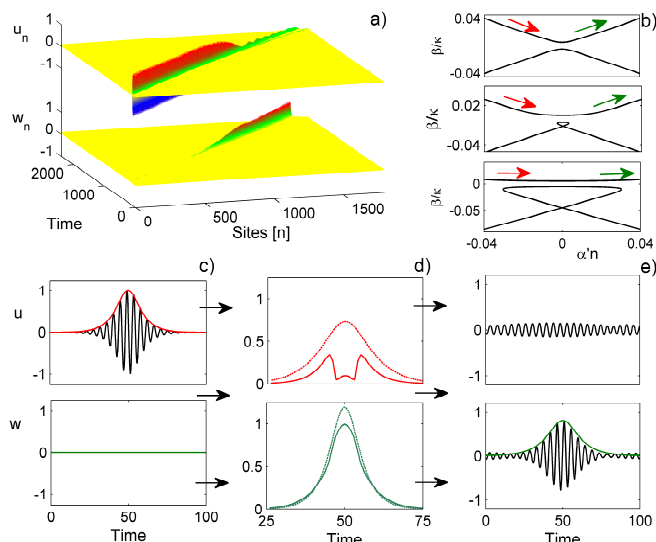


FIG. 3: a) surface plot of simulations on the initial model (13), (14) when unit amplitude soliton is injected in the upper chain. b) displays adiabatic dynamic associated with this process where the curves are taken solving quartic equation (7) and arrows indicate that soliton is switching to the lower chain. c)-d) graphs represent soliton LZ tunneling process. Particularly, in graph c) the shape of injected soliton with envelope function (10) in the upper chain is shown (while lower input is pinned). In graph d) we present resulting envelopes (solid lines) after tunneling derived from model Eqs. (5), (6). Dashed lines indicate constructed regular soliton envelopes (9) with the same width at half maximum as ones plotted by solid lines. e) shows formed output signal profiles followed from direct numerical simulations on (13) and (14) indicated by solid lines. Analytically computed envelope according to scheme (12) in the lower chain is given by dashed line, while in upper chain the envelope does not exist since the soliton does not form. The following parameters are used for the calculations: nonlinearity coefficient is  $k_3 = 0.015$ , while interchain constant takes the value  $k = 0.01$ , gradient is  $\alpha = 0.00008$  and we take carrier wavenumber  $p = \pi/2$ .

almost complete switch (Fig. 2(a) towards almost complete transmission (Fig. 2(b) according to general formula (8). However, for large wavenumbers  $p \approx \pi$  the correspondence is violated because of the reflection processes due to following reasons: for the mentioned carrier wavenumbers the wavepacket has a small group velocity and therefore Fresnell's reflection is in force, moreover as one goes closer to the Brillouin zone boundary, the wavepacket injected into the upper chain can not propagate in the same chain due to resonance mismatch. As a result tunneling is no more symmetric and there appear quantitative and qualitative differences compared with the original Landau-Zener model.

Turning back to the nonlinear case in frames of approximate description of Eqs. (5) and (6) we should deal with quartic equation for  $\beta$  level distribution (7). Corresponding curves in strongly nonlinear regime (defined by

condition  $r\mathcal{F} > \kappa$ ) are displayed in Fig. 3b and evidently there is definite asymmetry: Particularly, in case of small gradient constants  $\alpha$  adiabatic regime could be still realized injecting wavepacket into the upper chain, then the system follows the upper curve of the graph b) in Fig. 3, while injecting the wavepacket into the lower chain, the dynamics is always diabatic even in vanishing gradient case  $\alpha \rightarrow 0$  as it is evident from the lower curve of the same graph. Further we will consider only such strongly nonlinear cases  $r\mathcal{F} > \kappa$  and examining soliton splitting while passing through the tunneling region of the ladder.

In order to investigate soliton LZ tunneling process we employ a weakly nonlinear soliton solution in a single oscillator chain

$$G_n(\xi) = \frac{G \cos(\omega t - pn)}{\cosh(\xi)}, \quad \xi = \frac{n - vt}{\Lambda}, \quad (9)$$

where  $G$  and  $\Lambda$  are soliton amplitude and width, respectively, and the latter is defined from the relation  $1/\Lambda = G\omega\sqrt{3k_3/2}$ . Let us mentioned that the envelope of Expression (9) is associated [21] with exact one soliton solution of nonlinear Schrödinger equation.

Now we shall demonstrate all the procedures step by step on the particular examples presented in Figs. 3 and 4 where injection of the soliton into upper and lower chains, respectively, has been considered. In both cases we inject the soliton (9) with carrier wavenumber  $p = \pi/2$  (thus carrier frequency is  $\omega = \sqrt{2(1 - \cos p)} = \sqrt{2}$ ) and we take interchain coupling and nonlinearity constants as follows  $k = 0.01$ ,  $k_3 = 0.015$ , while the mass gradient in the tunneling region is  $\alpha = 0.00008$ . First we choose the input signal with a unit amplitude soliton (9) in the upper chain, i.e.  $G_0^U = 1$  and  $G_0^L = 0$ . Corresponding surface plot and level distribution is presented in Fig. 3a,b, while explicit form of the soliton shapes in upper and lower chains is presented in graph Fig. 3(c). This means, that according to the developed scheme of nonlinear LZ tunneling one has following values for the envelope variables  $A$  and  $B$  from (4) at the input  $n \rightarrow -\infty$ :

$$A(\xi, n \rightarrow -\infty) = \frac{1}{\cosh(\xi)}, \quad B(\xi, n \rightarrow -\infty) = 0. \quad (10)$$

For each value of variable  $\xi$  the input values of (10) undergo evolution following to the nonlinear LZ equations (5) and (6) getting after tunneling process the values  $A(\xi, n \rightarrow \infty)$  and  $B(\xi, n \rightarrow \infty)$  which do not have the regular soliton shape any more as it is evident from graph Fig. 3d (their shapes in both chains are plotted as solid lines). The obtained envelope distributions  $A(\xi, n \rightarrow \infty)$  and  $B(\xi, n \rightarrow \infty)$  could be now considered as initial conditions for the associated nonlinear Schrödinger equation, and the problem becomes exactly solvable [22–25]. In particular one is able to say whether the soliton will be formed or decayed. Moreover, one can predict the soliton amplitude and shape at the output of each chain explicitly in a good approximation.

In this connection, first of all, one should mention that it is crucial to determine characteristic amplitudes and widths of the obtained distributions  $A(\xi, n \rightarrow \infty)$  and  $B(\xi, n \rightarrow \infty)$ . Measuring their amplitudes in Fig. 3d we get following values:  $G_1^U = \text{Max}[A(\xi, n \rightarrow \infty)] = 0.995$  and  $G_1^L = \text{Max}[B(\xi, n \rightarrow \infty)] = 0.34$ , while measuring their width at half maximum we get:  $\Lambda_U = 11$  and  $\Lambda_L = 18$ . Next we should plot the regular soliton profile (9) characterized by the same width at half maximum. For our parameters the width of the regular soliton is defined from the relation  $1/\Lambda_0 = G\sqrt{3k_3}$  and thus the amplitudes of corresponding regular solitons are given by the following expressions:

$$G_2^U = \frac{\text{acosh}(2)}{\Lambda_U \sqrt{3k_3}} = 0.73, \quad G_2^L = \frac{\text{acosh}(2)}{\Lambda_L \sqrt{3k_3}} = 1.2. \quad (11)$$

The latter regular solitons are displayed in both chains by dashed lines in Fig. 3. Comparing now the amplitudes  $G_1^U$  and  $G_1^L$  with  $G_2^U$  and  $G_2^L$ , respectively, one can make definite predictions about formation of the solitons in each chain. In particular, as far as in the upper chain  $G_1^U/G_2^U < 1/2$  the soliton will not form at the output, while in the lower chain the soliton formation condition  $G_1^L/G_2^L > 1/2$  is satisfied and its amplitude could be computed approximately as follows:

$$G_L = 2G_2^L \left( \frac{G_1^L}{G_2^L} - \frac{1}{2} \right) = 0.8. \quad (12)$$

Then it is easy to recover the full shape of the solitons according to Exp. (9) and this gives excellent fit with the results of direct numerical simulations on initial set of equations (13) and (14) as is evident from Fig. 3e.

Now we proceed with the similar arguments in order to understand soliton spitting behaviour presented in Fig. 4a, where unit amplitude soliton (9) is injected into the lower chain. In this case the dynamics follows lower level line of Fig. 4b and therefore the process is strongly diabatic. As a result, the picture is quite different what we have seen in case of soliton injection into the upper chain (see Fig. 3). Following above developed procedure, one should measure characteristic amplitudes of solid line curves in Fig. 4d. We get following values:  $G_1^U = 0.805$ ,  $G_1^L = 0.6$ , while for their widths at half maximum we get:  $\Lambda_U = 5.6$  and  $\Lambda_L = 8$ . Next, as in previous case, we should plot the regular soliton profiles (9) characterized by the same width at half maximum and similar to (11) calculations give the regular soliton amplitude values  $G_2^U = 1.18$  and  $G_2^L = 0.82$ . Both associated regular solitons are displayed by dashed lines in Fig. 4. Comparing now the amplitudes  $G_1^U$  and  $G_1^L$  with  $G_2^U$  and  $G_2^L$ , respectively, one can conclude that soliton formation condition is fulfilled both in upper and lower chains and the solitons will form with amplitudes easily determined from the relation (12). Thus we get:  $G^U = 0.42$  and  $G^L = 0.37$ . Then one recovers solitons according to

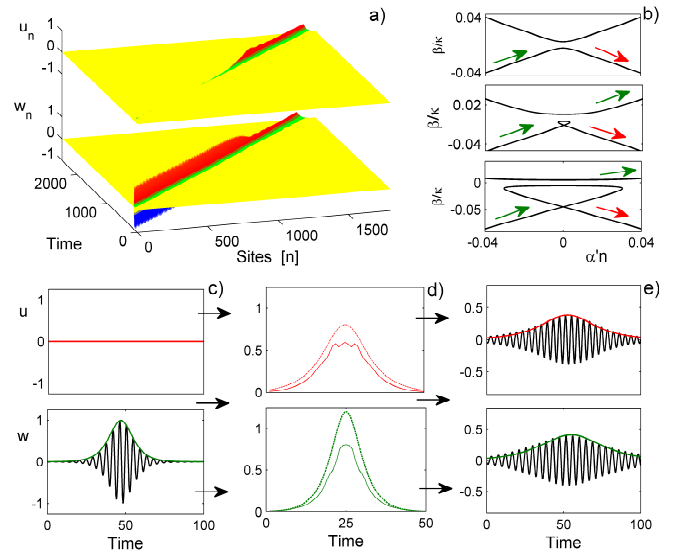


FIG. 4: a) Results of direct numerical simulations when unit amplitude soliton is injected into the lower chain. b) displays diabatic dynamic associated with the process and arrows indicate that part of the input soliton switches to the upper chain while another part stays in the same chain. c) the shape of injected soliton in the lower chain is shown (while upper input is pinned). d) represents resulting envelopes (solid lines) after tunneling derived from model Eqs. (5), (6). Dashed lines indicate constructed regular soliton envelopes (9) with the same width at half maximum as ones plotted by solid lines. e) shows formed output soliton profiles followed from direct numerical simulations on (13) and (14) indicated by solid lines. Analytically computed envelopes according to scheme (12) in the both chains are given by dashed lines. The parameters are the same as in Fig. 3.

Exp. (9) and compares with the results of direct numerical simulations that is done in Fig. 4e.

Concluding, we have identified soliton splitting phenomenon in gradiented weakly coupled chains of nonlinear oscillators as nonlinear Landau-Zener tunneling and made comparison between direct numerical simulations and simple analytical scheme. The correspondence between numerics and analytical justification becomes worse in case of large relative mass differences and/or small soliton propagation velocities. This is due Fresnel reflection which has not been taken into account. The investigations of interplay between Fresnel's reflection and Landau-Zener tunneling will be a subject of our further studies.

The authors acknowledge financial support from Georgian SRNSF (grant No FR/25/6-100/14). R. Kh. is supported in part by travel grants from Georgian SRNSF and CNR, Italy (grant No 04/24) and CNRS, France (grant No 04/01).

## APPENDIX

LZ tunneling region of our system is described by following equation:

$$\begin{aligned} m_0(1 - \alpha n)\ddot{u}_n &= k_1(u_{n+1} + u_{n-1} - 2u_n) + \\ &k_3(u_{n+1} - u_n)^3 + k_3(u_{n-1} - u_n)^3 + k(w_n - u_n) \\ m_0(1 + \alpha n)\ddot{w}_n &= k_1(w_{n+1} + w_{n-1} - 2w_n) + \\ &k_3(w_{n+1} - w_n)^3 + k_3(w_{n-1} - w_n)^3 + k(u_n - w_n) \end{aligned} \quad (13)$$

if we redefine parameters:  $k_3 \equiv \frac{k_3}{k_1}$ ,  $k \equiv \frac{k}{k_1}$  and introduce dimensionless time:  $t \equiv t\sqrt{\frac{k_1}{m_0}}$ , we obtain:

$$\begin{aligned} (1 - \alpha n)\ddot{u}_n &= (u_{n+1} + u_{n-1} - 2u_n) + \\ &k_3(u_{n+1} - u_n)^3 + k_3(u_{n-1} - u_n)^3 + k(w_n - u_n) \\ (1 + \alpha n)\ddot{w}_n &= (w_{n+1} + w_{n-1} - 2w_n) + \\ &k_3(w_{n+1} - w_n)^3 + k_3(w_{n-1} - w_n)^3 + k(u_n - w_n) \end{aligned} \quad (14)$$

Let us seek solutions of equations (14) as follows:

$$\begin{aligned} u_n &= \frac{A(\xi, \epsilon n)}{2} e^{i(\omega t - pn)} + C.C. \\ w_n &= \frac{B(\xi, \epsilon n)}{2} e^{i(\omega t - pn)} + C.C. \xi = \epsilon(n - vt) \end{aligned} \quad (15)$$

where  $\epsilon \ll 1$ ,  $v = \frac{\sin p}{w}$  and we suppose that  $\alpha n \lesssim \epsilon$ ,  $k \sim \epsilon$ ,  $k_3 \sim \epsilon$ .

In the zero approximation over  $\epsilon$ , we have a dispersion relation:

$$\omega^2 = 2(1 - \cos p) \quad (16)$$

while in the linear approximation over  $\epsilon$ , we get:

$$\begin{aligned} -i \frac{\partial A}{\partial n} &= \alpha' n A - \kappa(B - A) + 2r |A|^2 A \\ -i \frac{\partial B}{\partial n} &= -\alpha' n B - \kappa(A - B) + 2r |B|^2 B \\ \alpha' &= \frac{\alpha \omega^2}{2 \sin p}, \kappa = \frac{k}{2 \sin p}, r = \frac{3}{4}(\cos p - 1)^2 k_3 \end{aligned} \quad (17)$$

with a phase transformation  $A/B = A/B e^{i\kappa n}$ , we arrive to the equations:

$$\begin{aligned} -i \frac{\partial A}{\partial n} &= \alpha' n A - \kappa B + 2r |A|^2 A \\ -i \frac{\partial B}{\partial n} &= -\alpha' n B - \kappa A + 2r |B|^2 B \end{aligned} \quad (18)$$

This equation coincides with the equations (5)-(6) from the main text.

Now Let us define adiabatic levels. Substituting  $A/B = A/B e^{i(\beta + r\mathcal{F})n}$  into equations (18) (where  $\mathcal{F} = |A|^2 + |B|^2$  is constant for fixed  $\xi_0$ ), we get the following system of equations:

$$\begin{aligned} \beta A &= \alpha' n A - \kappa B + r(|A|^2 - |B|^2)A \\ \beta B &= -\alpha' n B - \kappa A - r(|A|^2 - |B|^2)B \end{aligned} \quad (19)$$

from (19) we can determine:

$$|A|^2 - |B|^2 = \frac{\alpha' n \mathcal{F}}{\beta - r\mathcal{F}} \quad (20)$$

combining (19)-(20), we have:

$$\begin{aligned} (\beta - \frac{\alpha' n \beta}{\beta - r\mathcal{F}})A + \kappa B &= 0 \\ \kappa A + (\beta + \frac{\alpha' n \beta}{\beta - r\mathcal{F}})B &= 0 \end{aligned} \quad (21)$$

equations (21) are linear homogenous equations for A and B. We have non-trivial solutions of (21), if:

$$(\alpha' n \beta)^2 = (\beta^2 - \kappa^2)(r\mathcal{F} - \beta)^2 \quad (22)$$

this quartic equations determine adiabatic levels  $\beta$  for fixed  $n$ .

- 
- [1] L. D. Landau, Phys. Z. Sowjetunion **2**, 46 (1932); G. Zener, Proc. R. Soc. London A **137**, 696 (1932).  
[2] B. P. Anderson and M. Kasevich, Science **282**, 1686 (1998).  
[3] M. Cristiani, O. Morsch, J. H. Muller, D. Ciampini, and E. Arimondo, Phys. Rev. A **65**, 063612 (2002).  
[4] H. Sanchis-Alepuz, Y. A. Kosevich, and J. Sanchez-Dehesa, Phys. Rev. Lett. **98**, 134301 (2007); L. Gutierrez, A. Diaz-de Anda, J. Flores, R. A. Mendez-Sanchez, G. Monsivais, and A. Morales, ibid. **97**, 114301 (2006).  
[5] R. Khomeriki and S. Ruffo, Phys. Rev. Lett. **94**, 113904 (2005).  
[6] H. Trompeter, T. Pertsch, F. Lederer, D. Michaelis, U. Streppel, A. Brauer, and U. Peschel, Phys. Rev. Lett. **96**, 023901 (2006).  
[7] F. Dreisow, A. Szameit, M. Heinrich, S. Nolte, A. Tunnermann, M. Ornigotti, and S. Longhi, Phys. Rev. A **79**, 055802 (2009).  
[8] A. Fratallocchi and G. Assanto, Opt. Express **14**, 2021 (2006).  
[9] H. Trompeter, W. Krolikowski, N. Neshev, S. Desyatnikov, A. A. Sukhorukov, Y. S. Kivshar, T. Pertsch, U. Peschel, and F. Lederer, Phys. Rev. Lett. **96**, 053903 (2006).  
[10] B. Wu and Q. Niu, Phys. Rev. A **61**, 023402 (2000).  
[11] J. Liu, L. Fu, B.-Y. Ou, S.-G. Chen, D. I. Choi, B. Wu, and Q. Niu, Phys. Rev. A **66**, 023404 (2002).  
[12] X.-Z. Liu, D.-P. Tian, B. Chong, Physica B, **490**, 1 (2016).  
[13] A. V. Shtyov, Phys. Rev. A **70**, 052708 (2004).  
[14] R. Khomeriki, Eur. Phys. J. D **61**, 193197 (2011).  
[15] R. Khomeriki and Sergej Flach, Phys. Rev. Lett., **116**, 245301 (2016).  
[16] M.A. Hasan, Y. Starosvetsky, A.F. Vakakis, L.I. Manevitch, Physica D, **252**, 46 (2013).  
[17] R. Khomeriki, Phys. Rev. A, **82**, 013839 (2010).  
[18] L. Chotorlishvili, R. Khomeriki, A. Sukhov, S. Ruffo, and J. Berakdar, Phys. Rev. Lett, **111**, 117202 (2013).

- [19] E. Fermi, J. Pasta, S. Ulam, and M. Tsingou, in *The Many- Body Problems*, edited by D. C. Mattis (World Scientific, Singapore, 1993); *The Fermi-Pasta-Ulam Problem: A Status Report*, edited by G. Gallavotti (Springer, New York, 2008).
- [20] A. Szameit, H. Trompeter, M. Heinrich, F. Dreisow, U. Peschel, T. Pertsch, S. Nolte, F. Lederer and A. Tünnermann, *New J. Phys.* **10**, 103020 (2008).
- [21] R. Khomeriki, *Physical Review E*, **65**, 026605 (2002).
- [22] T. Iizuka and M. Wadati, *J. Phys. Soc. Jpn.* **61**, 3077 (1992).
- [23] T. Iizuka, H. Amie, T. Hasegawa, and C. Matsuoka, *J. Phys. Soc. Jpn.* **65**, 3237 (1996).
- [24] J. Satsuma and N. Yajima, *Prog. Theor. Phys. Suppl.* **55**, 284 (1974).
- [25] L. Tkeshelashvili, *Phys. Rev. A* **86**, 033836 (2012).